Ingénierie des Systèmes d'Information
Vol. 31, No. 1, January, 2026, pp. 215-224
Journal homepage: http://iieta.org/journals/isi

Early Detection of Retinitis Pigmentosa from Pattern Electroretinography Signals Using Time–Frequency Analysis and Machine Learning

Mayada Alhamamy [1*], Mohammed Sabah Jarjees[1], W. Z. Wan Hasan[2]

[1] Department of Medical Instrumentation Techniques Engineering, Technical Engineering College of Mosul, Northern Technical University, Mosul 41001, Iraq
[2] Department of Electrical and Electronic Engineering, Universiti Putra Malaysia, Selangor 43400, Malaysia

Corresponding Author Email: mayada.fares@ntu.edu.iq

https://doi.org/10.18280/isi.310120

Received: 15 November 2025
Revised: 31 December 2025
Accepted: 15 January 2026
Available online: 31 January 2026

Keywords:
pattern electroretinography, retinitis pigmentosa, time–frequency analysis, discrete wavelet transform, continuous wavelet transform, machine learning, biomedical signal processing

ABSTRACT

Retinitis pigmentosa (RP) is a hereditary retinal disorder characterized by progressive degeneration of photoreceptor cells, ultimately leading to severe vision loss. Early detection of functional retinal abnormalities is essential for timely clinical intervention and effective disease management. Pattern electroretinography (PERG) provides an objective assessment of retinal ganglion cell activity and has been widely used for evaluating retinal function. This study proposes a machine learning–based framework for the early detection of RP using time-, frequency-, and time–frequency analyses of PERG signals. Temporal features describing amplitude and latency characteristics were first extracted from the time domain. Frequency-domain characteristics were then obtained using Fast Fourier Transform (FFT). To capture localized spectral–temporal variations in the signals, discrete wavelet transform (DWT) and continuous wavelet transform (CWT) were further employed for time–frequency feature extraction. Three machine learning classifiers—support vector machine (SVM), K-nearest neighbors (KNN), and quadratic discriminant analysis (QDA)—were evaluated to determine the most effective model for distinguishing RP patients from healthy subjects. Experimental results demonstrate that time–frequency features classified using QDA achieved the best performance, with an accuracy of 98.2%, outperforming models based solely on time-domain (94.5%) and frequency-domain (78.5%) features. These findings indicate that integrating temporal and spectral information significantly improves diagnostic performance and provides a reliable computational tool for early RP detection using PERG signals.

1. INTRODUCTION

Retinitis pigmentosa (RP) is a frequently encountered genetic retinal disease with an incidence of about 1 in 3,000 – 4,000 individuals around the world [1, 2]. The disease manifests during childhood or adolescence, starting with night blindness then progressing to the narrowing of vision until it reaches total blindness [3, 4]. In the early stages, there are mild or asymptomatic symptoms, and commonly used clinical examinations, such as fundus examination or visual field test reveal no changes [5]. Therefore, electroretinography (ERG), particularly pattern electroretinography (PERG), is an effective tool for the early detection of retinal ganglion cell dysfunction, as it accurately measures electrical function even in the absence of structural changes or impaired vision [6]. Recent research using AI-based automated systems on retinal imaging demonstrated great diagnostic accuracy, suggesting the use of intelligent techniques to PERG signal analysis for early RP detection [7].

PERG signals in RP patients are characterized by decreased amplitude and delayed latency, especially in the N35, P50, and N95 components. Most previous clinical studies have focused on analyzing signals in the time domain only (such as wave amplitude and peak time) [8], but these indicators alone may not reflect the subtle changes that occur in the early stages of the disease. Therefore, advanced analysis methods such as the Fast Fourier transform (FFT), the discrete wavelet transform (DWT), and the continuous wavelet transform (CWT) have been used to detect the spectral and temporal components of biomarkers [9], as they have the ability to distinguish non-stationary changes in the signal with higher accuracy [10]. The recent years (2016–2025) have witnessed significant progress in the analysis of ERG signals using multidomain techniques. In 2016, the integration of the FFT and the CWT was employed to analyze Full-field Electroretinogram (ffERG) signals, illustrating the capability to identify alterations in latency and amplitude in individuals with RP [11]. Subsequently, in 2022, nonlinear methods were applied to improve classification accuracy, achieving satisfactory results of approximately 90% [12]. However, these results were limited to the ffERG signals and limited samples. From 2023 to 2024, research has concentrated on integrating PERG or Optical Coherence Tomography Angiography (OCTA) signals with artificial intelligence (AI) methodologies, showing satisfactory efficacy in differentiating between disease states. Nonetheless, these are confined to advanced

disease stages and limited data sets [13, 14]. In 2025, researchers used machine learning (ML) algorithms to look at multifocal electroretinography (mfERG) signals and got accuracy rates of over 95% [15]. However, their focus was on structural changes in the retina rather than functional aspects. Despite the significant progress in this research, most studies still rely on ffERG or mfERG signals and are limited to single-domain analysis (time or frequency only), without comprehensive integration of time-frequency information. Most studies do not address PERG signals or focus on the early stages of the disease. Therefore, this study aims to develop an integrated approach for analyzing the hybrid (time-frequency) characteristics of PERG signals for early detection of RP using accurate ML classifiers. The proposed approach is based on analyzing signals in the time, frequency, and time-frequency domains using DWT and CWT transforms, then classifying the extracted features with support vector machine (SVM), K-nearest neighbors (KNN) and quadratic discriminant analysis (QDA) algorithms to identify the most effective indicators in distinguishing between healthy and diseased individuals, enhancing the potential of this method in early diagnosis of disease.

2. MATERIAL AND METHODS

Data from typical PERG recordings were obtained from the PhysioNet database, which includes the archive of a research project at the Institute of Applied Ophthalmobiology (IOBA) of the University of Valladolid in Spain. The database comprises a well-characterized cohort of clinically diagnosed RP patients and healthy control participants. Signals were recorded according to internationally approved protocols from the International Society for Clinical Electrophysiology of Vision ISCEV standards, adhering to quality and reliability standards, and data were collected from 2003 to 2022. A sampling rate of 1700 Hz was used over a 150-ms time window for each recording. The project obtained the necessary ethical approvals, and informed consent forms were signed by participants [16].

High, having a clinical impression by an expert diagnosis using diagnostic labeling in the dataset. As described in the metadata, three different independent clinical diagnoses could have been assigned to each subject (diagnosis1, diagnosis2, and diagnosis3). These were based on evaluations by senior ophthalmology specialists. Subjects were considered to have RP only if RP was documented in diagnostic fields specifically, and control subjects came from records with 'Normal' recorded as the absence of retinal pathology.

Specific clinical staging information of RP (i.e., early stage, intermediate stage, advanced stage) was not available in this dataset and couldn't be directly adopted into the analysis. However, the fact that measurable transient PERG responses were available suggests that these recordings reflect functional stages where retinal electrophysiological activity can still be measured. or absent in advanced RP, the method proposed focuses on identifying functional retinal dysfunctions at a stage where electrophysiological responses are not necessarily extinguished. Since PERG responses are typically severely attenuated or absent in advanced RP, the proposed approach focuses on detecting functional retinal dysfunction at stages where electrophysiological responses are still present.

The study included 47 participants with RP (24 females and 23 males) and 47 healthy controls (24 females and 23 males). The age ranged from 9 to 81 years in the RP group (mean ± SD: 36.2 ± 18 years) and from 4 to 86 years in the control group (mean ± SD: 35.7 ± 20 years). Two PERG recordings were available for each participant, corresponding to the right and left eyes. However, the analysis was performed at the individual level rather than the eye level; therefore, features extracted from both eyes were combined to form a single representation per participant.

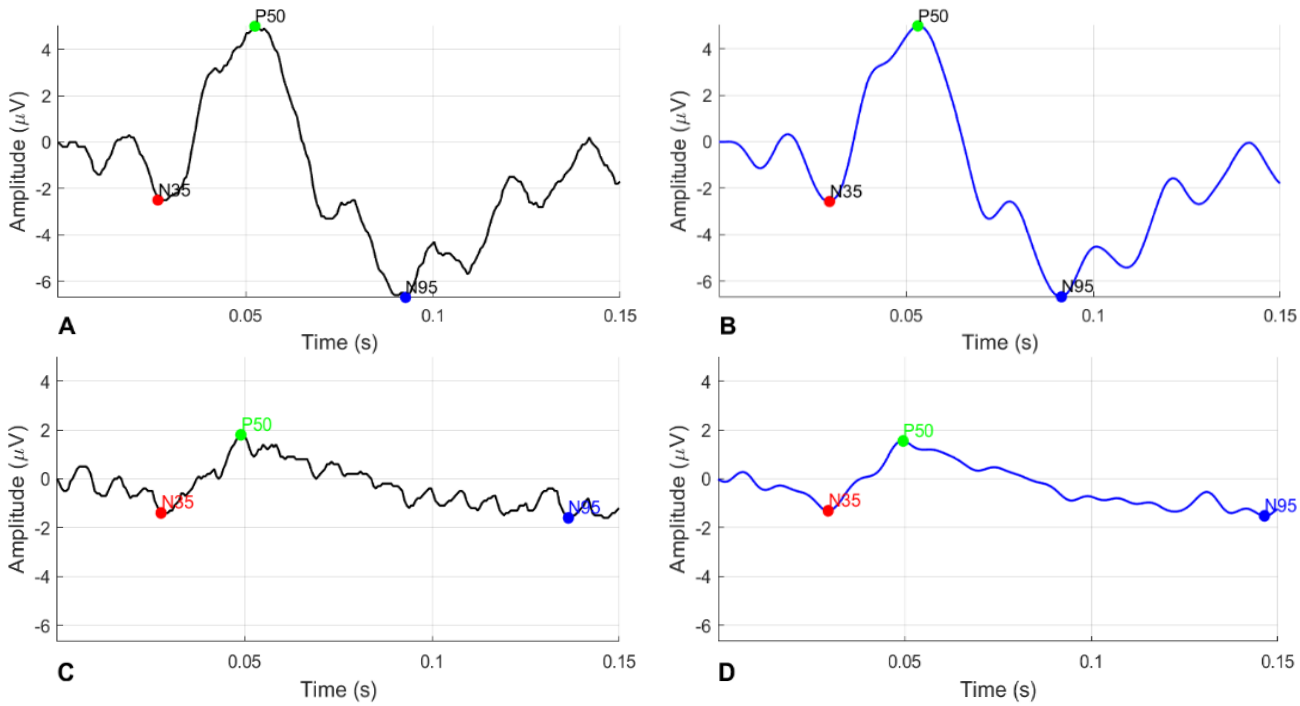

Figure 1. The raw and filtered ERG signals in both a healthy retina and a case of RP, with subplots (A–B) representing the healthy case and (C–D) representing the diseased case
Note: ERG = electroretinography; RP = retinitis pigmentosa.

Structural imaging data, such as optical coherence tomography (OCT), were not available in the dataset. Although visual acuity measurements were included in the metadata, they were not used in the classification process. Consequently, the analysis focused exclusively on functional retinal responses derived from PERG signals. Inclusion criteria consisted of the availability of high-quality transient PERG recordings with complete metadata and clear diagnostic labeling as either RP or normal. No additional exclusion criteria were applied. All signals were further filtered with a fourth-order Butterworth low-pass filter (0–100 Hz) to remove high-frequency noise while preserving the overall shape of the signal. No high-pass or baseline correction was applied since the original recordings did not contain baseline drift. Zero-phase filtering (filtfilt) was used to maintain the timing and amplitude of the PERG waveform peaks, as shown in Figure 1.

Then, data augmentation methods were applied only to the training set by adding a small amount of random noise 0.5% of the maximum signal amplitude and applying a slight random scaling ± 2% of the original signal amplitude to each eye. After this technique, the dataset was expanded to 141 samples per group, resulting in a total of 282 healthy and affected samples. This augmentation increases the variability of training data and improves model generalization while the test set remained unchanged, ensuring evaluation on real, unseen data. Once recorded, signals were measured in the time domain; principal components such as the first negative peak (N35), maximum positive amplitude (P50), and the most negative peak (N95) were extracted, and 12 features were identified. MATLAB was used to perform an FFT in the frequency domain and then extract 8 features, such as peak frequency, peak power, and band power. In the time–frequency domain, a total of 52 features from CWT and DWT coefficients were extracted. using the same software. Feature selection was performed separately for each domain. Only features that showed statistically significant differences between the RP and control groups.

2.1 Fourier transform analysis of PERG signals

Fourier Analysis (FA) is a technique that operates entirely in the frequency domain, decomposing a time-domain signal into its constituent frequency components that collectively reconstruct the original signal [17]. The transformation from the time domain to the frequency domain is achieved using the Fourier Transform (FT):

$$X(f) = \int_{-\infty}^{+\infty} x(t) \cdot e^{-2j\pi ft}\, dt \qquad (1)$$

where, *X(f)* is the signal in the frequency domain and x(t) is the signal in the time domain. In this study, the FFT within the MATLAB environment was used to analyze the PERG signals and extract the frequency features, such as peak frequency, peak power, and frequency band power, which help in distinguishing between healthy individuals and those with RP, as shown in Figure 2.

Although the FFT is efficient at characterizing the spectral structure of a signal, it lacks temporal information that captures the moment of frequency change, limiting its accuracy in analyzing non-stationary signals such as PERG signals. Therefore, the analysis was later complemented by time-frequency analysis techniques to provide a combined representation of time and frequency, enabling a more accurate characterization of dynamic changes in the signal.

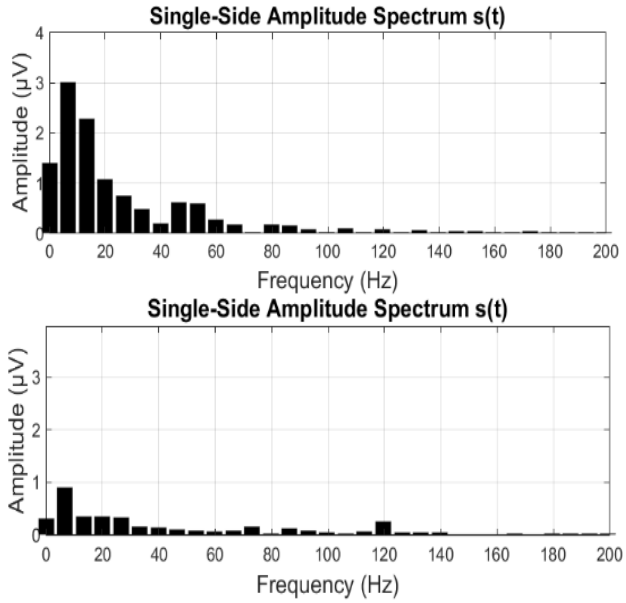

Figure 2. FFT-based single-sided amplitude spectra of PERG signals for a normal subject (top) and a patient with RP (bottom)
Note: FFT = Fast Fourier Transform; PERG = pattern electroretinography; RP = retinitis pigmentosa.

2.2 Time-frequency analysis

One powerful tool for capturing the spectral modulations of a signal in time is time-frequency analysis. It is effective for studying non-stationary biomedical signals that change over time [18, 19]. WT is often used in both ways, to enlarge the information extracted and also to refine and obtain better results [20]. Various transformations have been employed to produce features indicating change in the signal over time and frequency.

Wavelet transforms are broadly of two types, CWT and DWT [18, 21]. CWT is a multi-purpose, flexible analytical tool. They are a great method to analyze non-stationary time series data. They use a variable-length analysis window that adapts to frequency. This allows for high resolution at low frequencies, while short windows are used for high-frequency analysis, providing a more accurate and time-varying assessment [22]. In the analysis of ERG signals, the Mexican Hat Wavelet (MHW), the second derivative of a Gaussian function, was used as the mother wavelet due to its similarity to the shape of the ERG signal compared to other wavelets such as Haar, Morlet, and Daubechies. According to previous studies on ERG signals, the components include f0 (summed activity of stimulated photoreceptor cells), f1 (activity of cylinder photoreceptors), and f2 (activity of cone photoreceptors) [23]. All of these frequency components are time-matched to the main wavelets of the ERG. MHW allows for precise detection and timing of temporal fluctuations, helping to distinguish normal from abnormal signals. The MHW is defined by:

$$MHW(t,\tau,\sigma) = \frac{1}{\sqrt{2\pi}}\left[1-\left(\frac{t-\tau}{\sigma}\right)\right]\cdot e^{-\frac{1}{2}\left(\frac{t-\tau}{\sigma}\right)^2} \qquad (2)$$

It is a continuous, non-orthogonal signal, characterized by a small number of regular oscillations that begin to form and then gradually fade away over the desired time period [22].

The second kind of transform is the DWT, which is characterized by high processing speed and high accuracy that made it suitable for some applications such as signal classification and data compression. Thus, DWT descriptors should be added to the analysis of retinal functionality in terms of time domain [24]. particularly when difficult cases are being examined. DWT is essentially a set of high-pass and low pass filters with up-sampling and down-sampling operations. In this study, DWT was applied to the signal across five analysis levels. At each level, the signal is divided into two bands: a low-pass filter and a high-pass filter. The low-pass part contains richer information about the signal. DWT generates coefficients to represent the signal across multiple frequency levels [17]. From these coefficients, features such as energy (which represents the amount of energy in the signal) and entropy (which reflects the randomness of the data) are extracted. These features are used in pattern recognition, data compression, and noise removal. The DWT coefficient equation is given by the following Eq. (3) [17].

$$DWT(j,k) = \frac{1}{\sqrt{2j}} \int_{-\infty}^{+\infty} x(t)\, \psi\left(\frac{t - 2^j k}{2^j}\right) dt \qquad (3)$$

2.3 Classification and validation

Initially, the classification process was performed using subject-level data separation to prevent information leakage between training and testing sets. All recordings from the same subject were kept within the same subset to ensure independence between training and test data. The dataset was divided into 80% for training (226 signals) and 20% for testing (56 signals), ensuring a balanced evaluation of model performance on unseen subjects and reducing the risk of overfitting during training. We consider that the selection of classifiers and their parameter values was not arbitrary; these were experimental and applications made through MATLAB Classification Learner. Several preliminary tests were conducted to evaluate the performance of different models, and the classifiers demonstrating the highest accuracy SVM, KNN, and QDA were adopted. All parameters were optimized within the application to achieve the best performance. After identifying the optimal parameters, the classifiers were implemented in MATLAB scripts, where 10-fold cross-validation repeated 10 times was applied to the full dataset for each classifier to assess performance reliably and reduce variability due to random data partitioning. QDA does not require extensive hyperparameter tuning, and its default parameters were used while performance was evaluated using the same cross-validation procedure. This cross-validation method divides the dataset into k subsets, using each subset in turn as the training and test set. The model's performance is evaluated for each subset, and at the end of the process, k-test results are averaged to provide a stable estimate of performance [15]. For every fold, the dataset was split into training and testing sets at a 9:1 proportion, and repeating the cross-validation ten times further reduces the influence of random data partitioning on the results. In this proposed work, to more efficiently classify the time-domain signal dataset, solve complex problems, and capture nonlinear patterns [25], the linear kernel function of the SVM algorithm was used, with automatic kernel scaling (KernelScale = auto) and a regularization coefficient of 1 (BoxConstraint = 1). QDA, which relies on estimating discrete variance matrices for each class (DiscrimType = 'quadratic'), was used for hybrid domain classification due to its ability to model complex data distributions. A final classifier was used for frequency domain features, employing a distance-based KNN approach (NumNeighbors = 5, Standardize = true, and 100 learners in the set), since these frequency features can be considered inherently nonlinear and unevenly distributed across samples. Comparisons were performed using the Mann–Whitney test due to non-normal distributions, with Bonferroni correction applied for multiple comparisons as well. Data are reported as median (interquartile range, IQR) to accurately summarize central tendency and variability. Unadjusted p-values were initially computed for all comparisons. Adjusted p-values (adj_p) were used to determine whether the observed differences between healthy and patient groups were statistically significant. To reinforce that, effect sizes (Cohen's d) were calculated to quantify the magnitude of the differences, offering insight into the findings' practical or therapeutic importance beyond their statistical significance. This combination strategy ensures that the reported differences are both statistically valid and impactful.

3. RESULTS

This section focuses on presenting and analyzing the results obtained after the model completed the classification process in detail. The performance metrics, including sensitivity, precision, accuracy, F1 score, recall, and receiver operating characteristic area under the curve (ROC-AUC) score. The analysis also highlights the most important time-domain, frequency-domain, and time-frequency- features that contribute to the discrimination between groups. Finally, the obtained results are compared with those reported in previous studies to place them in a broader research context and confirm the effectiveness of the proposed approach in improving the diagnostic ability of PERG features in detecting retinal abnormalities in patients with RP.

3.1 Time domain result

The data from 282 balanced samples were analyzed between normal individuals and patients with RP. The results Pertinent component and eye-specific differences for both PERG amplitudes and latencies were evident, indicating a heterogeneous retinal dysfunction. The effect size (Cohen's d) was calculated as the standardize difference between healthy controls and RP patients. PERG changes in RP patients showed distinct component- and eye-related patterns. For the right eye, effects were observed more strongly in terms of reduction in amplitude than in latency, with P50 showing the largest effect (adj_p = 2.57×10^{-10}, d = 0.67) and N35 amplitudes showing a moderate but significant difference (adj_p = 0.0019, d = 0.57), while N95 amplitudes did not remain significant after Bonferroni correction. Latency prolongation was limited to N95 (adj_p = 0.0116, d = −0.32), while N35 and P50 latencies did not reach significance after multiple comparison correction. In the left eye, P50 amplitude remained significantly reduced (adj_p = 0.0011, d = 0.42), N35 amplitude did not show a significant difference (adj_p = 1, d = −0.20), whereas N95 amplitude showed a statistically significant difference (adj_p = 3.29×10^{-5}, d = −0.23). Latency differences were statistically significant for N35, P50, and

N95, with moderate effect sizes for N35 (adj_p = 0.0149, d = 0.48) and N95 (adj_p = 1.65 × 10^{-7}, d = 0.52), and a smaller effect for P50 (adj_p = 0.0083, d = 0.28), indicating component-specific temporal processing alterations. indicating component-specific temporal processing alterations. The comparative effect size analysis demonstrated that amplitude features tended to offer better discrimination than latency characteristics in general, with P50 amplitude in the right eye emerging as the most robust marker of functional impairment. The presence of inter-eye asymmetry in PERG parameters is consistent with the intrinsically heterogeneous and not synchronous course of RP, as we already know, at least during early and intermediate stages. The function of the two eyes may deteriorate unequally, resulting in eye-specific amplitude and latency differences. This model is consistent with known pathophysiological processes, where early photoreceptor degeneration and secondary remodeling of inner retinal circuitry can produce measurable electrophysiological alterations before overt structural loss occurs. Similar interocular differences have been consistently reported in previous electrophysiological and clinical studies [26]. The detailed quantitative findings are presented in Table 1, while Figure 3 illustrates the group-wise differences in PERG amplitudes and latencies between healthy participants and RP patients.

3.2 Frequency domain result

The data from 282 balanced samples were analyzed between normal individuals and patients with RP. After performing frequency band analysis, the power in both the low-frequency (1–7 Hz) and mid-frequency (7–20 Hz) bands showed a significant reduction in RP patients compared with healthy subjects in both eyes (adjusted $p < 0.001$ for all bands). This reduction indicates a loss of retinal signal energy and impaired signal transmission from photoreceptors to bipolar cells, consistent with the known pathophysiology of RP [6]. Regarding peak frequency, a statistically significant difference was observed in the right eye (adjusted $p = 0.0237$), reflecting increased variability in RP patients despite identical median values between groups. In contrast, no significant difference was found in the left eye (adjusted $p = 1$), which may reflect interocular variability or asymmetric disease progression. Peak power was significantly reduced in RP patients in both eyes (adjusted $p < 0.001$), confirming a marked weakening of the dominant spectral component of the ERG signal. Overall, these findings demonstrate that RP alters the spectral structure of the ERG signal, characterized by reduced frequency-band power and peak power, along with changes in dominant frequency. Detailed statistical results are presented in Table 2, and Figure 4 illustrates the comparisons using separate plots with clearly defined measurement units.

Table 1. Statistical comparison of ERG features between healthy controls and RP patients

Feature	Normal	RP	p_value	Effect_Size_d	adj_p
RE_N35_amp	-0.170 (-0.547–0.013)	-0.370(-0.692–-0.090)	0.000161439	0.567520126	0.00193727
RE_P50_amp	3.400 (1.880–5.272)	1.390 (0.510–2.257)	2.13904E-11	0.674133093	2.56685E-10
RE_N95_amp	-2.450(-3.790–-1.208)	-2.070(-3.635–-0.838)	0.177893443	-0.113945152	1
LE_N35_amp	-0.240 (-0.520–-0.020)	-0.210 (-0.530–0.107)	0.261982188	-0.20143752	1
LE_P50_amp	2.970 (1.672–4.290)	1.510 (0.818–3.562)	9.18672E-05	0.416886827	0.001102406
LE_N95_amp	-2.870 (-4.302– -1.410)	-1.250 (-2.670–0.003)	2.73873E-06	-0.225479504	3.28648E-05
RE_N35_lat	0.009 (0.003–0.013)	0.008 (0.003–0.010)	0.018447506	0.309813831	0.221370074
RE_P50_lat	0.053 (0.049–0.056)	0.054 (0.024–0.066)	0.869945641	0.109074372	1
RE_N95_lat	0.104 (0.096–0.120)	0.117 (0.102–0.136)	0.000965938	-0.317014419	0.01159126
LE_N35_lat	0.011 (0.004–0.020)	0.008 (0.004–0.010)	0.001243397	0.484479496	0.014920765
LE_P50_lat	0.051 (0.049–0.054)	0.055 (0.023–0.081)	0.000692412	-0.275759613	0.008308939
LE_N95_lat	0.102 (0.095–0.111)	0.117 (0.102–0.128)	1.37552E-08	-0.517347693	1.65062E-07

Note: ERG = electroretinography; RP = retinitis pigmentosa.

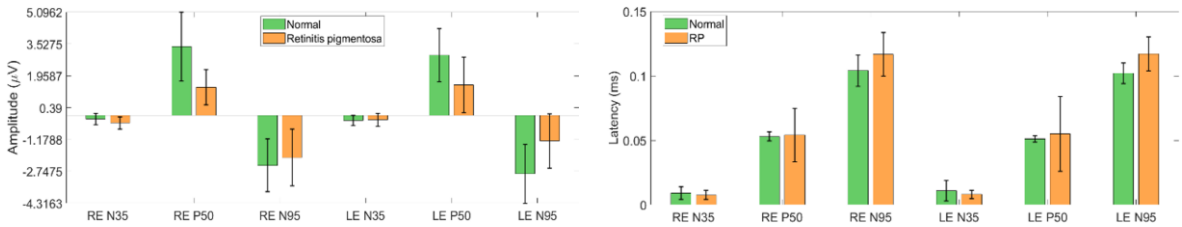

Figure 3. Comparison of time-domain PERG features between healthy participants and participants with RP in the right eyes (RE) and left eyes (LE)

Bars represent group median values, and error bars indicate half of the IQR (IQR/2) for amplitudes (μV) and latencies (ms) of the N35, P50, and N95 components.

Note: PERG = pattern electroretinography; RP = retinitis pigmentosa.

Table 2. Differences in spectral indicators between healthy and participants with RP individuals

Feature	Normal	RP	p_value	Effect_Size_d	adj_p
R_bp_1_7	24.613(10.010-52.078)	4.769 (2.501–13.892)	1.90889E-12	0.468101319	1.52711E-11
L_bp_1_7	21.373 (8.604–49.135)	8.339 (2.724–22.019)	4.12178E-08	0.321464229	3.29742E-07
R_bp_7_20	0.642 (0.303–1.093)	0.068 (0.016–0.240)	9.15425E-19	0.586577827	7.3234E-18
L_bp_7_20	0.560 (0.286–1.111)	0.089 (0.022–0.230)	2.06598E-17	0.454496306	1.65278E-16
R_peakFreq	6.641 (6.641–6.641)	6.641 (6.641–13.281)	0.002965001	0	0.023720007
L_peakFreq	6.641 (6.641–6.641)	6.641 (6.641–6.641)	0.55305288	0	1
R_peakPower	0.279 (0.149–0.555)	0.074 (0.026–0.264)	1.24962E-13	0.471544529	9.99693E-13
L_peakPower	0.254 (0.133–0.536)	0.084 (0.030–0.192)	3.18448E-14	0.211953123	2.54758E-13

Note: RP = retinitis pigmentosa.

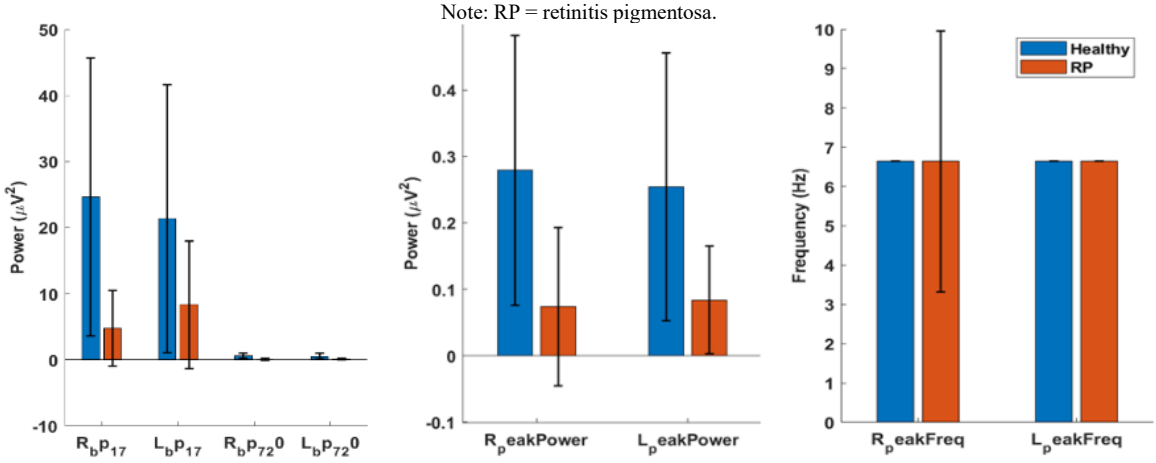

Figure 4. Comparison of frequency-band power (1–7 Hz and 7–20 Hz), peak frequency (Hz), and peak power (μV²) between healthy subjects and patients with RP

Note: RP = retinitis pigmentosa; IQR = interquartile range.
Values are presented as median ± IQR.

3.3 Time–Frequency domain result

The data from 282 balanced samples were analyzed between normal individuals and patients with RP. Comparisons were performed using the Mann–Whitney test due to non-normal distributions, with Bonferroni correction applied for multiple comparisons. In DWT analysis, all power levels (0–4) showed statistically significant differences between groups. Level 0 showed the largest difference (adj_p = 2.6179E-08), levels 1 and 2 showed moderate differences (adj_p = 0.0109 and 0.0003547, respectively), and levels 3 and 4 showed high differences (adj_p = 1.5198E-06 and 1.0619E-06, respectively), indicating statistically significant differences in both low- and high-frequency components in RP patients, although the effect size was small for levels 1-4 CWT analysis revealed significantly lower frequency (f0, f1, f2) and temporal (t0, t1, t2) feature values in RP patients compared to healthy controls after Bonferroni correction, with most features remaining statistically significant based on adjusted p-values. This reduction indicates alterations in both the spectral and temporal organization of PERG signals, reflecting impaired retinal function associated with progressive photoreceptor degeneration. One feature (R_cwt_f0) did not remain significant after adjustment (adj_p = 0.054544241), suggesting relative preservation of this component. These findings are consistent with the results presented in Tables 3 and 4 and Figure 5, where heat maps and box plots illustrate clear differences in the temporal and frequency-domain characteristics between healthy subjects and RP patients.

Table 3. Median and IQR of PERG power across DWT levels (0–4)

Feature	Normal	Retinitis Pigmentosa	p_value	Effect_Size_d	adj_p
0	11838.87(7092.20–16585.53)	19343.47(12814.198–25872.7)	5.23584E-09	-0.985	2.61792E-08
1	472.570(76.268–868.87)	688.55 (293.28–1083.81)	0.002178914	-0.302	0.010894572
2	187.920(-34.974–410.81)	107.660(-15.986–231.31)	7.09497E-05	0.161	0.000354748
3	69.765(-78.191–217.72)	41.825(1.810–81.840)	3.03964E-07	0.059	1.51982E-06
4	72.650(-45.682–190.98)	25.235 (-0.059–50.529)	2.12392E-07	0.134	1.06196E-06

Note: IQR = interquartile range; PERG = pattern electroretinography; DWT = discrete wavelet transform.

Table 4. Comparison of feature statistics between healthy and RP patients

Feature	Normal	Retinitis Pigmentosa	p_value	Effect_Size_d	adj_p
R_cwt_f0	17.350 (6.675–68.155)	10.940 (3.495–24.648)	0.004545	0.358	0.054544241
L_cwt_f0	24.100 (6.862–75.725)	6.880 (2.333–17.517)	2.41643E-07	0.423	2.89971E-06
R_cwt_f1	21.210 (5.135–62.995)	8.060 (3.360–20.405)	7.99315E-05	0.476	0.000959178
L_cwt_f1	21.370 (2.422–55.080)	5.330 (1.775–16.008)	1.45096E-05	0.437	0.000174115
R_cwt_f2	12.000 (4.600–66.390)	5.030 (1.770–13.465)	2.37E-07	0.54	2.84366E-06
L_cwt_f2	13.060 (2.598–30.258)	3.200 (0.982–11.095)	2.57186E-07	0.361	3.08623E-06
R_cwt_t0	6.190 (2.515–37.412)	2.720 (0.940–8.112)	4.3535E-08	0.664	5.2242E-07
L_cwt_t0	8.690 (2.333–29.962)	2.310 (0.518–8.385)	3.31203E-08	0.311	3.97443E-07
R_cwt_t1	3.760 (1.110–18.495)	1.490 (0.502–5.025)	9.73923E-07	0.408	1.16871E-05
L_cwt_t1	5.080 (1.515–21.803)	1.840 (0.610–5.355)	3.00493E-06	0.334	3.60592E-05
R_cwt_t2	4.180 (0.770–9.180)	1.190 (0.398–3.485)	7.73E-06	0.299	9.27303E-05
L_cwt_t2	4.490 (0.882–17.462)	1.250 (0.440–3.322)	3.14629E-06	0.277	3.77554E-05

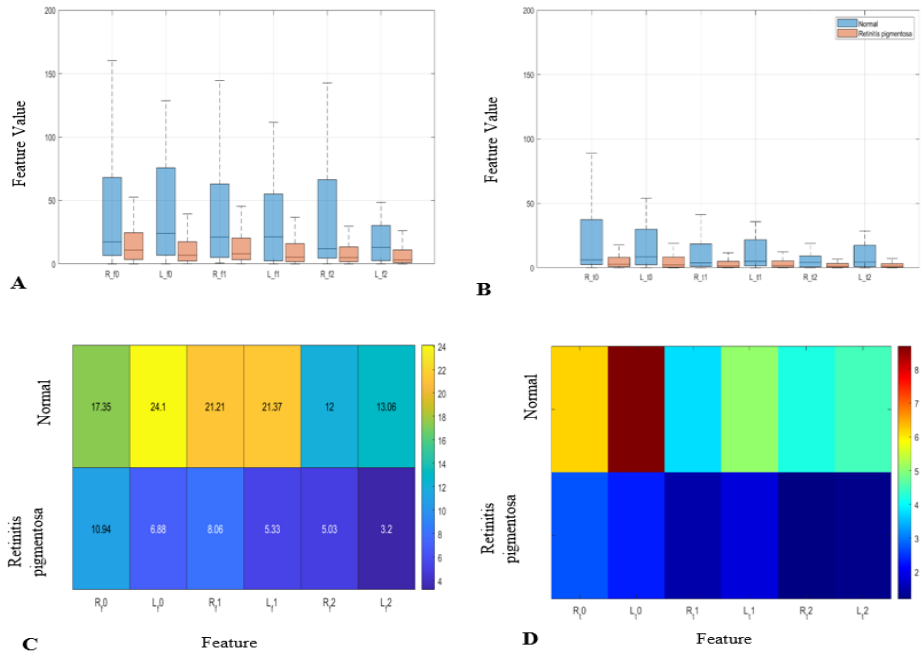

Figure 5. Boxplots and heat maps illustrate the differences between RP patients and healthy controls in temporal (t0, t1, t2) and frequency (f0, f1, f2) features for both eyes

These plots highlight the variability in values and differences between the two groups, outliers, and the distribution of data across different levels of analysis.
Note: RP = retinitis pigmentosa.

4. STATISTICAL VALIDATION

To express the reliability and reproducibility of observed differences, effect sizes (Cohen's d) were calculated, which suggested moderate-to-large separations of healthy from RP individuals (d = 0.4–0.7). 95% confidence intervals (CIs) were calculated based on repeated cross-validation with bootstrap (1,000 iterations). The hybrid time–frequency model showed the best stability with narrow CIs for accuracy (98.2%, [95% CI: 95.4–99.6]) and AUC 0.93, [0.90–0.96], indicating reliable and statistically robust performance of the model in the generalization sense. Together, these analyses support the reliability of the proposed time–frequency using the QDA framework for distinguishing early RP from normal retinal responses.

5. DISCUSSION

The classification results in this study demonstrate that the effectiveness of PERG signals in early detection of RP clearly depends on the type of analysis domain used. In the time domain, latency and amplitude parameters of N35, P50, and N95 waves were analyzed in both eyes of healthy subjects and patients with retinitis pigmentosa. As shown in Table 1 and Figure 3, the PERG responses showed a significant amplitude reduction and latency delay in the RP group compared to healthy subjects, with the test accuracy reaching 94.5, indicating the sensitivity of temporal parameters, particularly P50 and N95 waves, to early functional changes in the retina. These components are associated with the neural activity of ganglion and macular cells, and changes in their amplitude or latency are well-known early signs of retinal dysfunction. These findings are consistent with those of Zhang et al. [27], who reported that electrophysiological responses such as Visual Evoked Potential (VEP) showed reduced amplitudes and delayed latencies in RP, reflecting impaired neural activity in the visual pathway. Although the timing and intensity of retinal responses are also important, time-domain results do not reveal how signal energy is distributed at various frequencies. As such, frequency domain analysis was employed to go further in the investigation of PERG spectral features and to search for potential changes in retinal synchronization. As shown in Table 2 and Figure 4, Analysis of the frequency characteristics of the PERG signals revealed clear differences between RP patients and the healthy control group. Spectral power in the lower bands was higher in healthy controls, while the patient group showed lower peak power. The results also showed that the overall classification accuracy based only on spectral parameters was about 78.5%, highlighting the limitations of relying on spectral measures such as dominant frequency or power bands. Because PERG signals are non-stationary and contain localized temporal variations, spectral analysis alone may overlook transient disturbances. These results are consistent with those of Arsiwalla et al. [28], who reported reduced cone function and flicker response amplitude in RP patients when analyzed using frequency-based ERG measurements. Therefore, the frequency domain can be considered an effective method for measuring the spectral degradation of retinal signals, complementing time-domain results, and supporting early diagnosis.

The dominant frequencies derived from the waveform transformation analysis (f0, f1, and f2) are actually the main component frequencies, and each can indicate the activities of different structures in the visual system, depending on their temporal order. f0 refers to the combined activities of photoreceptors, while f1 and f2, the higher frequencies, are associated with the role of f1 photoreceptors in rods and f2 photoreceptors in cones and their unique properties. The results of the waveform transformation of the ERG signal using both time- and frequency-domain waveform transformations were statistically different between the RP patients and healthy controls. DWT analysis revealed that

power levels at all analytical levels (0–4) were significantly affected in patients, with level 0 exhibiting the largest and most statistically significant difference between groups. Since level 0 corresponds to the approximation coefficients of the DWT, it represents the low-frequency components of the ERG signal, which are associated with slow retinal potentials and sustained photoreceptor activity. This observed decrease in low-frequency power indicates a substantial impairment in the functional integrity of photoreceptors and inner retinal cells responsible for generating slow, sustained retinal responses in RP patients. A moderate but also significant difference was found in the intermediate levels (levels 1 and 2). These modifications probably mirror higher signal perturbation and lower synchronization between neurons instead of immediate physiological events. In contrast, amplitudes of levels 3 and 4 also had a significant difference, suggesting disturbance in frequency bands, which contribute to the fine temporal structure of the PERG waveform. Overall, the DWT findings indicate that retinal dysfunction in RP is not confined to a single temporal scale but affects both low- and higher-frequency components of the ERG signal, with the most pronounced impairment occurring in the low-frequency domain. CWT analysis supported the findings mentioned above, showing significantly lower (f0-f2) and time (t0-t2) coefficients in patients compared to healthy controls in most cases. This decrease in CWT coefficients reflects the increased instability and loss of structure in retinal function associated with photoreceptor degeneration. Heat maps and box plots (Figure 5) also indicated that the spread of CWT values in RP subjects was greater, reflecting inter-subject variance in the progression of disease. One characteristic (R_cwt_f0) was not significant anymore after Bonferroni correction (adj_p = 0.0545), which indicates a certain degree of conservation of this feature. Integration of temporal and spectral features allows a more comprehensive analysis of retinal activity, with test accuracy reaching 98.2% and a cross-validation accuracy of over 92.9%. These waveforms allow us to isolate short-lived oscillatory events and energy fluctuations associated with early dysfunctions in the inner and outer retinal layers. These results are consistent with previous studies, in which Ebdali et al. [29] reported that wavelet-based analysis provides superior sensitivity to FFT in detecting subtle changes in retinal responses, confirming that time- and time-frequency measurements more accurately capture early signatures of disease compared to frequency-based methods alone. Furthermore, the model performance was stable with 10-fold cross-validation with an accuracy as high as 93.95%, compared to the SVM model on time characteristics (accuracy: 90.38%) and the KNN model on frequency characteristics (accuracy: 78.45%), indicating consistency in model strength QDA over different data subsets. In Table 5, the comparative analysis with classifiers over different analysis domains clearly indicated that the time–frequency features achieved the highest testing accuracy and cross-validation accuracy. Furthermore, Figure 6 shows the best model's performance employing time-frequency characteristics, with the ROC curve (Left) confirming significant discriminative capacity (AUC = 0.93) and the confusion matrix (Right) demonstrating reliable classification between normal and RP samples. It should be noted that this study is cross-sectional and primarily aimed at distinguishing RP patients from healthy controls. Therefore, while the results demonstrate the effectiveness of PERG signal analysis for detecting the disease, they do not provide direct information about disease progression. Future longitudinal studies are needed to evaluate the potential of these features for monitoring functional retinal changes over time. A comparative summary with representative ERG-based and ML studies is provided in Table 6, highlighting the relative strengths and limitations of the proposed approach.

Table 5. Classification accuracy results for different analysis domains

Metric	Time Domain	Frequency Domain	Time–Frequency Domain
Classifier	SVM	KNN	QDA
Test Acc	94.50	78.5	98.21
Accuracy Cross Validation	89	79.01	92.92
Recall	89.3	100	98.2
Precision	95.2	73	96.5
F1 Score	94	0.84	98.25
AUC	0.98	0.84	0.93
Standard 10-Fold CV Acc	90.38	78.45	93.95

Note: SVM = support vector machine; KNN = K-nearest neighbors; QDA = quadratic discriminant analysis; AUC = area under the curve.

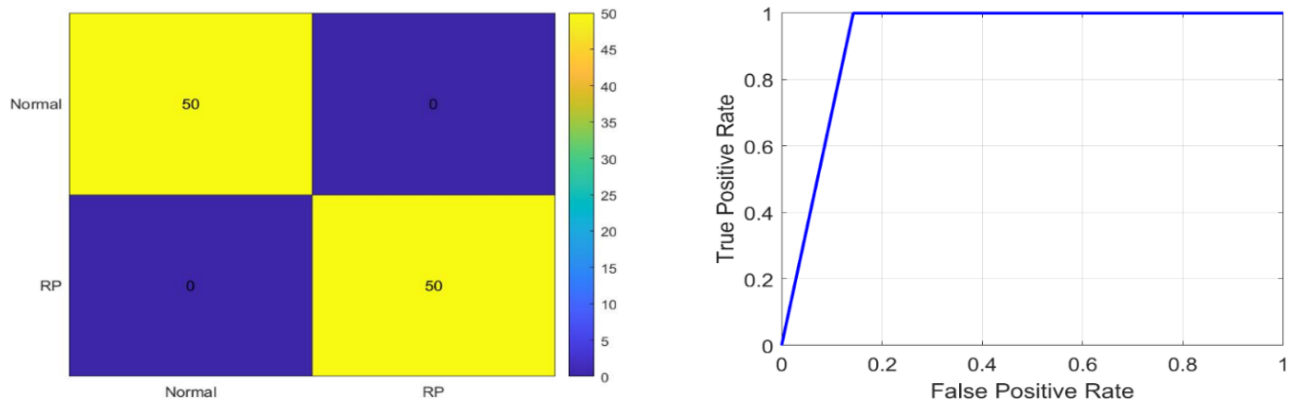

Figure 6. Performance evaluation of the best time-frequency model. (Left) ROC curve demonstrating the model's discriminative performance (AUC = 0.93). (Right) Confusion matrix showing the classification of Normal vs. RP samples

Note: ROC = receiver operating characteristic; AUC = area under the curve.

Table 6. Summary of previous ERG-based studies in RP

Ref.	Signal / Method	Subjects (n)	Performance / Accuracy	Key Findings	Limitations
[11]	ffERG, FFT + CWT	18 RP + 20 Controls	Not reported	Latency increased, amplitude decreased, and significant frequency changes.	Small sample; frequency loss in advanced RP.
[28]	ffERG, PERG, mfERG, OCT, VEP, fMRI	26 patients	Not reported	OCT & VEP detected decline; ERG unrecordable in late RP.	Small fMRI sample.
[12]	ffERG + nonlinear mapping	28 RP + 32 Controls	88–91% (nonlinear classifier)	Nonlinear features improved classification.	Short ERG signals; variability.
[13]	PERG + OCTA	25 RP + 25 Controls	Not reported	PERG amplitudes decreased; vessel density decreased.	Small sample; PERG sensitivity limited.
[14]	PERG + AI (Claude-3)	46 (20 Controls, 13 RP, 13 CRD)	100% (AI pathology detection)	PERG features effective for RP/CRD discrimination.	Limited dataset.
[15]	mfERG + ML (Naive Bayes, SVM, LR	77 RP + 19 Controls	99% (binary), 82% (multiclass)	Excellent RP vs control classification.	Validation needed on larger datasets.
Our Study	PERG	47RP+47 Controls	94.5% (time), 78.5% (frequency), 98.2% (time–frequency)	Integration of time–frequency PERG features provided superior sensitivity to early retinal dysfunction and robust classification using QDA.	Cross-sectional design; binary classification only; no external validation.

Note: ERG = electroretinography; RP = retinitis pigmentosa; ffERG = full-field electroretinography; FFT = Fast Fourier Transform; CWT= continuous wavelet transform; PERG = pattern electroretinography; mfERG = multifocal electroretinography; OCT = optical coherence tomography; VEP = visual evoked potential; fMRI = functional magnetic resonance imaging; CRD = cone-rod dystrophy; PERG = pattern electroretinography; LR = logistic regression; QDA = quadratic discriminant analysis.

6. CONCLUSIONS

Although it is difficult to analyze retinal function in patients with RP, based on experimental results and data analysis this study showed that by using a combination of time domain analysis and frequency domain analysis of PERG signals with wavelet based techniques (DWT & CWT), it was possible to detect subtle pathological changes resulting from early retinal dysfuncion. While both amplitude and effect time are useful diagnostic indicators, are most reliable when combined with frequency characteristics. In summary, the developed method in this study offers a potential and the basis for the development of advanced clinical tools for the early detection and monitoring of RP in future clinical trials. Although the results are promising, the relatively small dataset and lack of external validation remain limitations. Future studies should include larger and independent datasets to further verify the model's clinical applicability.

REFERENCES

[1] Huang, Z.Y., Liang, L.N., Li, Y.M., Xu, K., Li, X.Y. (2022). Genetic, environmental and other risk factors for progression of retinitis pigmentosa. International Journal of Ophthalmology, 15(5): 828-837. https://doi.org/10.18240/ijo.2022.05.21

[2] Qi, X.Y., Mi, C.H., Cao, D.R., Chen, X.Q., Zhang, P. (2024). Retinitis pigmentosa and stem cell therapy. International Journal of Ophthalmology, 17(7): 1363-1369. https://doi.org/10.18240/ijo.2024.07.22

[3] Narayan, D.S., Wood, J.P.M., Chidlow, G., Casson, R.J. (2016). A review of the mechanisms of cone degeneration in retinitis pigmentosa. Acta Ophthalmologica, 94(8): 748-754. https://doi.org/10.1111/aos.13141

[4] Amato, A., Wongchaisuwat, N., Lamborn, A., Everett, L., Yang, P., Pennesi, M.E. (2023). Early macular involvement in non-syndromic retinitis pigmentosa. In Macular Diseases-An Update. https://doi.org/10.5772/intechopen.1003723

[5] Hamel, C. (2006). Retinitis pigmentosa. Orphanet Journal of Rare Diseases, 1: 40. https://doi.org/10.1186/1750-1172-1-40

[6] Thompson, D.A., Bach, M., McAnany, J.J., Šuštar Habjan, M., Viswanathan, S., Robson, A.G. (2024). ISCEV standard for clinical pattern electroretinography (2024 update). Documenta Ophthalmologica, 148(2): 75-85. https://doi.org/10.1007/s10633-024-09970-1

[7] Sheet, S.S.M., Tan, T.S., As'ari, M.A., Hitam, W.H.W., Sia, J.S.Y. (2022). Retinal disease identification using upgraded CLAHE filter and transfer convolution neural network. ICT Express, 8(1): 142-150. https://doi.org/10.1016/j.icte.2021.05.002

[8] Haraguchi, Y., Chiang, T.K., Yu, M.Z. (2023). Application of electrophysiology in non-macular inherited retinal dystrophies. Journal of Clinical Medicine, 12(21): 6953. https://doi.org/10.3390/jcm12216953

[9] Nair, S.S., Paul Joseph, K. (2014). Wavelet based electroretinographic signal analysis for diagnosis. Biomedical Signal Processing and Control, 9: 37-44. https://doi.org/10.1016/j.bspc.2013.09.008

[10] Alhamamy, M.F., Jarjees, M.S., Hasan, W.Z.W. (2025). Electroretinography: A comparative study of modalities and analytical approaches with partial integration of OCT findings. NTU Journal of Engineering and Technology, 4(4): 39-58. https://doi.org/10.56286/v3x8ga74

[11] Ebdali, S., Hashemi, B., Jafarzadehpour, E. (2017). Comparing the variation of time and frequency components of electroretinogram in patients with retinitis

pigmentosa and healthy individuals. Journal of Mazandaran University of Medical Sciences, 26(145): 110-121.
[12] Bakhshi, S., Behbahani, S., Daftarian, N. (2021). Application of a mapping method in the analysis of electroretinogram in patients with retinitis pigmentosa. Seminars in Ophthalmology, 37(3): 351-357. https://doi.org/10.1080/08820538.2021.1967411
[13] Altas, F.B., Doguizi, S., Onder, E.G., Sekeroglu, M.A. (2023). Anatomical and functional reflections of vascular changes in retinitis pigmentosa. Research Square. https://doi.org/10.21203/rs.3.rs-3463934/v1
[14] Aykut, A., Akgün, B., Sezenöz, A.S., Sevik, M.O., Sahin, Ö. (2024). Diagnosing retinal disorders with artificial intelligence: The role of large language models in interpreting pattern electroretinography data. Journal of Health Sciences and Medicine, 7(5): 538-542. https://doi.org/10.32322/jhsm.1506378
[15] Karaman, B., Öner, A., Güven, A. (2025). Early detection and staging of retinitis pigmentosa using multifocal electroretinogram parameters and machine learning algorithms. Physical and Engineering Sciences in Medicine, 48(3): 1185-1205. https://doi.org/10.1007/s13246-025-01577-3
[16] Fernández, I., Cuadrado-Asensio, R., Larriba, Y., Rueda, C., Coco-Martín, R.M. (2024). A comprehensive dataset of pattern electroretinograms for ocular electrophysiology research. Scientific Data, 11(1): 551. https://doi.org/10.1038/s41597-024-03857-1
[17] Behbahani, S., Ahmadieh, H., Rajan, S. (2021). Feature extraction methods for electroretinogram signal analysis: A review. IEEE Access, 9: 116879-116897. https://doi.org/10.1109/ACCESS.2021.3103848
[18] Lin, Z., Chen, J.D.Z. (1996). Advances in time-frequency analysis of biomedical signals. Critical Reviews in Biomedical Engineering, 24(1): 1-72. https://doi.org/10.1615/CritRevBiomedEng.v24.i1.10
[19] Kheirati Roonizi, A., Sassi, R. (2024). ECG signal decomposition using Fourier analysis. EURASIP Journal on Advances in Signal Processing, 2024(1): 79. https://doi.org/10.1186/s13634-024-01171-x
[20] Gosala, B., Kapgate, P.D., Jain, P., Chaurasia, R.N., Gupta, M. (2023). Wavelet transforms for feature engineering in EEG data processing: An application on Schizophrenia. Biomedical Signal Processing and Control, 85: 104811. https://doi.org/10.1016/j.bspc.2023.104811
[21] Nguyen, T.D., Nguyen, P.D. (2024). Improvements in the wavelet transform and its variations: Concepts and applications in diagnosing gearbox in non-stationary conditions. Applied Sciences, 14(11): 4642. https://doi.org/10.3390/app14114642
[22] Barraco, R., Adorno, D.P., Brai, M., Tranchina, L. (2014). A comparison among different techniques for human ERG signals processing and classification. Physica Medica, 30(1): 86-95. https://doi.org/10.1016/j.ejmp.2013.03.006
[23] Erkaymaz, O., Yapici, I.S., Arslan, R.U. (2021). Effects of obesity on time-frequency components of electroretinogram signal using continuous wavelet transform. Biomedical Signal Processing and Control, 66: 102398. https://doi.org/10.1016/j.bspc.2020.102398
[24] Gauvin, M., Chakor, H., Koenekoop, R.K., Little, J.M., Lina, J.M., Lachapelle, P. (2016). Witnessing the first sign of retinitis pigmentosa onset in the allegedly normal eye of a case of unilateral RP: A 30-year follow-up. Documenta Ophthalmologica, 132(3): 213-229. https://doi.org/10.1007/s10633-016-9537-y
[25] Vuckovic, A., Gallardo, V.J.F., Jarjees, M., Fraser, M., Purcell, M. (2018). Prediction of central neuropathic pain in spinal cord injury based on EEG classifier. Clinical Neurophysiology, 129(8): 1605-1617. https://doi.org/10.1016/j.clinph.2018.04.750
[26] Tucker, L., Marmoy, O.R., Handley, S.E., Thompson, D.A. (2024). Ambient lighting alters pattern electroretinogram P50 peak time and spatial sensitivity. Documenta Ophthalmologica, 149(2): 77-86. https://doi.org/10.1007/s10633-024-09984-9
[27] Zhang, M., Ouyang, W., Wang, H., Meng, X., Li, S., Yin, Z.Q. (2021). Quantitative assessment of visual pathway function in blind retinitis pigmentosa patients. Clinical Neurophysiology, 132(2): 392-403. https://doi.org/10.1016/j.clinph.2020.11.023
[28] Arsiwalla, T.A., Cornish, E.E., Nguyen, P.V., Korsakova, M., Ali, H., Saakova, N., Fraser, C.L., Jamieson, R.V., Grigg, J.R. (2020). Assessing residual cone function in retinitis pigmentosa patients. Translational Vision Science & Technology, 9(13): 29. https://doi.org/10.1167/tvst.9.13.29
[29] Ebdali, S., Hashemi, B., Hashemi, H., Jafarzadehpur, E., Asgari, S. (2018). Time and frequency components of ERG responses in retinitis pigmentosa. International Ophthalmology, 38(6): 2435-2444. https://doi.org/10.1007/s10792-017-0748-3

NOMENCLATURE

x(t)	Time-domain PERG signal
X(f)	Frequency-domain representation of the signal
f	Frequency variable
t	Time variable
ψ(t)	Mother wavelet function
MHW (t, τ, σ)	Mexican Hat Wavelet
τ	Time-shift parameter
σ	Wavelet scale parameter
j	Decomposition level in DWT
k	Translation index in DWT
DWT(j,k)	Discrete Wavelet Transform coefficients
CWT(t,f)	Continuous Wavelet Transform coefficients

Greek symbols

π	Mathematical constant
ω	Angular frequency

Subscripts

0	Level-0 wavelet features
1	Level-1 wavelet features
2	Level-2 wavelet features
3	Level-3 wavelet features
4	Level-4 wavelet features
R	Right eye
L	Left eye